

# *Advanced gate control system for power MOSFET switching losses reduction with complete switching sequence control*

*Rok Vrtovec, Janez Trontelj*

*University of Ljubljana, Faculty for Electrical Engineering, Ljubljana, Slovenia*

**Abstract:** To meet strict EMC requirements for power electronics applications driving an inductive load, it is often necessary to mitigate current and voltage transition slopes. Using the conventional MOSFET control method, the slope mitigation is commonly performed by modifying a series gate resistance, which results in high switching losses, long turn-on and turn-off delays and long final gate charging and discharging durations affecting the overall application efficiency. In order to improve this, a novel MOSFET control method is developed and presented in this paper. It enables a complete control over all intervals of the switching sequences utilizing the gate current shaping principle. Switching losses, delays and final gate charging and discharging durations can be kept as low as possible, as the method allows to mitigate only the critical transition. The design of the system allows its implementation in a broad spectrum of applications regardless of the current or voltage rating and with a minimal impact on the application design. The paper presents the detailed description of the proposed system operation and its realization as an integrated circuit. The efficiency measurements of the conventional and the advanced gate control methods are reported as well, showing significant advantages of the proposed system.

**Keywords:** Power MOSFET switching behavior; advanced gate control; gate current shaping; switching losses reduction; EMC in power electronics

# *Napredno krmiljenje vrat močnostnih MOSFET tranzistorjev za zmanjševanje preklopnih izgub z nadzorom nad celotno preklopno sekvenco*

**Izveček:** Za doseganje elektromagnetne skladnosti moramo v močnostni elektroniki pri napravah z induktivnim bremenom pogosto zmanjšati naklon toka ali napetosti med preklopi. Pri konvencionalni krmilni metodi to storimo s spreminjanjem serijske upornosti v vratih MOSFET tranzistorja. Slednje se odraža v povečanju preklopnih izgub, podaljšanju zakasnitev vklopa in izklopa ter podaljšanju trajanja končnega polnjenja in praznjenja vrat. Našteto zmanjšuje zmogljivost celotne naprave. Navedene pomanjkljivosti konvencionalne metode ublažimo z uporabo nove napredne krmilne metode, ki je predstavljena v tem članku. Deluje na principu spreminjanja toka, ki teče v vrata MOSFET tranzistorja ter omogoča nadzor nad dogajanjem v vsakem intervalu preklopne sekvence. Ker lahko na tak način omilimo le kritični naklon, sistem omogoča vzdrževanje minimalnih preklopnih izgub, zakasnitev in trajanj končnega polnjenja in praznjenja vrat. Sistem je zasnovan tako, da ga lahko vgradimo v širok spekter naprav, ne glede na napetostno ali tokovno zmogljivost in z minimalnim poseganjem v zasnovano same naprave. V članku je detajlno opisano delovanje predstavljenega sistema ter njegova realizacija v obliki integriranega vezja. Predstavljene so tudi meritve učinkovitosti konvencionalne in napredne kontrole vrat. Rezultati so občutno boljši v primeru uporabe predstavljenega sistema.

**Ključne besede:** Preklopi močnostnega MOSFET tranzistorja; napredno krmiljenje vrat; oblikovanje toka v vrata tranzistorja; zmanjševanje preklopnih izgub; EMC v močnostni elektroniki

\* Corresponding Author's e-mail: rok.vrtovec@fe.uni-lj.si

## 1 Introduction

The tradeoff between switching losses and electromagnetic emissions is often of great concern during the design of power electronic applications with an inductive load. Fast transitions of voltage and current at power switch (in this paper we are focusing on power MOSFETs) cause excessive emissions and oscillations, while slow transitions cause significant switching losses. To meet strict EMC requirements, slopes must often be limited, which is obviously done at the expense of increased switching losses.

Power MOSFETs are commonly driven via series gate resistor ( $R_g$ ). Transition slopes are adjusted by changing  $R_g$  value but such approach is not the most effective. The problem is that changing  $R_g$  resistance influences all intervals of the switching sequence instead of mitigating only the critical transition that is responsible for emissions. This produces excessive switching losses, introduces long turn-on and turn-off delays and extends final gate charging and discharging durations. To improve this process, a different gate control method should be used to allow control over transition in each interval of the switching sequence independently.

Several papers [1–10] report improvements of the conventional control method with a gate resistor or propose entirely new control approaches that differ in functionality, complexity, efficiency and cost.

For example, the methods presented in [1], [2], [4], [7] focus only on the mitigation of turn-off voltage overshoot and the following oscillations, which are often an issue especially among IGBT circuits. Papers [5], [8] introduce the combined control over turn-off voltage and turn-on current transition. The latter is usually of great concern, as the current slope impacts reverse recovery severity, it may induce oscillation and it strongly impacts the emissions rate. The method [9] focuses on the acceleration of turn-on voltage fall and minimization of the turn-off delay. The most comprehensive approaches are reported by Rose [3], Park [6] and Lobsiger [10] demonstrating current and voltage transition control during the turn-on and the turn-off. None of the presented methods, however, addressed control over the whole duration of the switching sequence.

The presented control methods are based on significantly different principles for the operating point detection of the controlled MOSFET (or IGBT), which is an essential part of any advanced control method. Certain methods [2], [6], [7], [10] use capacitor or special differentiator circuit connected to the transistor drain (or collector) terminal. Despite being simple and low-cost, such approach may be susceptible to noise [4] and os-

cillations that potentially mask the actual voltage transition resulting in an inappropriate control procedure. On the other hand, methods [3], [4], [6], [10] exploit intrinsic inductances from the physical circuit to detect the current transitions. Such system may be found difficult to implement, taking into account diverse layout topologies, current slopes and ratings.

Gate control approach as presented in this paper aims to enable control over transitions in all intervals of the switching sequences and to use such operating point detection principle that allows system implementation in various applications regardless of voltage or current ratings and with a minimal impact on the circuit layout design.

Presented system is also a subject of PCT patent application.

Paper is organized in the following order: section 2 presents the inductive load switching sequence, switching losses and EMC overview and provides an explanation about the conventional gate control drawbacks; section 3 describes the concept of the proposed gate control system; section 4 presents system realization as an integrated circuit; section 5 presents system measurements, results and discussion, while section 6 concludes the paper.

## 2 Switching sequences, switching losses and EMC

A short insight into a well known switching behaviour of a MOSFET with a clamped inductive load is given first in order to present switching losses and electromagnetic emission (EM) generation and to underline the importance of the advanced gate control introduction.

A clamped inductive load circuit, presented in Figure 1, is comprised of MOSFET  $M_1$ , inductive load ( $L_{load}$ ), free-wheeling diode ( $D_{fwd}$ , which is the intrinsic diode of permanently closed MOSFET  $M_2$ ), driving circuit ( $V_{gg}$  and  $R_g$ ), MOSFET  $M_1$  intrinsic capacitances ( $C_{gs}$  and  $C_{gd}$ ) and supply voltage source  $V_{bat}$ . The corresponding switching waveforms of  $M_1$  turn-on and turn-off sequences are shown in Figure 2 [11]. Just before the  $t_{or}$  the initial conditions in the circuit are as follows:  $v_{gs}=0$  and  $v_{ds}=0$ , so  $M_1$  is switched-off ( $i_d=0$ ); due to previous excitations, inductor  $L_{load}$  drives current  $I_0$  through  $D_{fwd}$  ( $i_{fwd}=I_0$ ), and since  $D_{fwd}$  is forward-biased,  $v_{ds}$  equals  $V_{bat}$ .

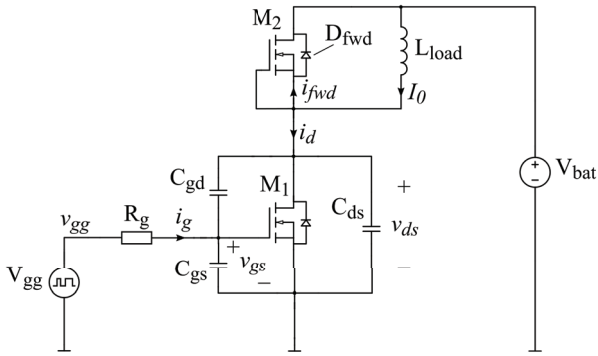


**Figure 1:** Clamped inductive load circuit

The turn-on sequence starts with the interval  $T_1$  (turn-on delay) at  $t=t_{o'}$  when  $V_{gg}$  turns-on ( $v_{gg}=V_{gg}$ ) and starts charging  $C_{gs}$  (Figure 2a). As  $v_{gs}$  reaches the threshold voltage  $V_{th}$  at the beginning of the interval  $T_2$ ,  $M_1$  starts conducting (Figure 2b) and taking over the load current  $I_0$  from  $D_{fwd}$ . When  $i_d$  rises to  $I_0$ ,  $i_{fwd}$  falls to zero, so  $D_{fwd}$  can be reverse-biased; the reverse-recovery process takes effect manifesting as  $M_1$  drain current overshoot. During the whole interval  $T_2$ , the forwardly biased  $D_{fwd}$  clamps  $v_{ds}$  to  $V_{bat}$  level. In the interval  $T_3$ ,  $v_{ds}$  drops as  $C_{gd}$  is discharged (Figure 2c). The total current from  $V_{gg}$  is now diverted to  $C_{gd}$ , causing  $v_{gs}$  to remain constant at the Miller plateau ( $V_{\mu}$ ). After  $v_{ds}$  drops to  $V_{ds,on}$  (a consequence of  $M_1$  channel resistance),  $C_{gs}$  starts charging again and  $v_{gs}$  is rising again towards  $V_{gg}$  in  $T_4$ . The turn-on is thus accomplished [11] [12].

The turn-off occurs in a similar manner. It begins with  $V_{gg}$  going low at  $t=t_{o'}$ , followed by a turn-off delay interval  $T_4'$ , in which  $v_{gs}$  falls to Miller plateau, as  $C_{gs}$  is discharged (Figure 2e). Beyond  $v_{gs}=V_{\mu}$ , further  $C_{gs}$  discharging requires drain current reduction, which is impossible at that moment, since  $D_{fwd}$  is reverse biased ( $V_{bat}>v_{ds}$ ) and cannot take over load current ( $I_0$ ) yet. Therefore,  $v_{ds}$  rises first in  $T_3'$  (Figure 2g). When  $v_{ds}$  meets  $V_{bat}$ ,  $I_0$  can eventually be diverted to  $D_{fwd}$ , so  $M_1$  drain current ( $i_d$ ) falls in  $T_2'$  (Figure 2f). At  $v_{gs}=V_{th}$ ,  $M_1$  closes ( $i_d=0$ ,  $i_{fwd}=I_0$ ) and only  $v_{gs}$  remains to drop to zero in  $T_1'$ , thus terminating turn-off sequence [11].

The review of the switching sequences shows that the current ( $i_d$ ) transitions in  $T_2$  and  $T_2'$  occur at the full voltage ( $v_{ds}$ ) on  $M_1$ . Similarly, voltage ( $v_{ds}$ ) transitions in  $T_3$  and  $T_3'$  occur at the maximum drain current. This results in high power dissipation,  $p_{sw}=i_d \cdot v_{ds}$ . The integrals of  $p_{sw}$  over  $T_2$  and  $T_3$  for turn-on (1) and over  $T_2'$  and  $T_3'$  for turn-off (2) determine the turn-on ( $E_{sw,on}$ ) and turn-off ( $E_{sw,off}$ ) switching losses (Figure 2d and h) [11] [12].

$$E_{sw,on} = \int_{T_2, T_3} p_{sw}(t) dt = \frac{1}{2} I_0 V_{bat} (T_2 + T_3) \quad (1)$$

$$E_{sw,off} = \int_{T_2', T_3'} p_{sw}(t) dt = \frac{1}{2} I_0 V_{bat} (T_2' + T_3') \quad (2)$$

The dissipated energy, manifested as heat, is the root cause of several engineering challenges. Most importantly, it is necessary to provide adequate heat sinking, which often results in a bulky and expensive design and presents a limit for the application implementation. Moreover, elevated application temperature results in increased degradation rate of assembly components and impact general system reliability. As switching losses may present an important source of heating, their minimization is of great concern [13].

It is also well established that current and voltage transitions in  $T_2$ ,  $T_2'$  and  $T_3$ ,  $T_3'$  are the main source of electromagnetic emissions in power applications. High  $di/dt$  and  $dv/dt$  rates in conjunction with inductive and capacitive coupling cause conducted (and indirectly also radiated) differential (DM) and common mode (CM) emissions. Moreover,  $di/dt$  and  $dv/dt$  could excite oscillations and overshoots in resonant circuits (formed by parasitic inductances and capacitances), producing additional emissions and affecting the system reliability. There are several mechanisms available to mitigate emissions and oscillations (to meet EMC standards), each with its own trade-offs. One possibility is obviously to decrease  $di/dt$  and  $dv/dt$  rates (i.e. extend intervals  $T_2$ ,  $T_3$ ,  $T_2'$  and  $T_3'$ ) and eliminate the emissions origin, but at the expense of additional switching losses. We can furthermore tweak layout or insert additional components, such as snubber circuits or blocking capacitors, which usually involves a lot of prototyping and has only limited effect. Another possibility is the implementation of CM and DM filters, which is an effective but bulky and expensive solution. Most designs require to utilize all of the above, each in the scope of its own trade-offs and affected application characteristics [13][14]. On the other hand, any improvement of the described mechanisms eases the application design and boosts its efficiency.

This paper presents one of such improvements, which deals with the MOSFET control circuit and increases slope adaptation mechanism efficiency. The main drawback of the conventional method employing a series gate resistor  $R_g$  is that increasing the gate circuit resistance in order to reduce critical current or voltage slopes prolongs all intervals in corresponding switching sequence. First, it causes excessive switching losses in  $T_2$ ,  $T_2'$ ,  $T_3$  or  $T_3'$  as it extends both current and voltage transitions. Moreover, an extension of  $T_1$  and  $T_4$  has a negative impact on applicability of some control algorithms, as it requires longer dead-times and in turn also produces higher diode  $D_{fwd}$  losses [12]. Extension of  $T_4$  or  $T_1'$  affects the system reliability in terms of the unintentional turn-on / turn-off immunity.

Introduction of the advanced gate control system presented in this paper, which allows setting the duration of each interval of the switching sequence separately, extends the margins where slope adaptation effectively improves the application efficiency.

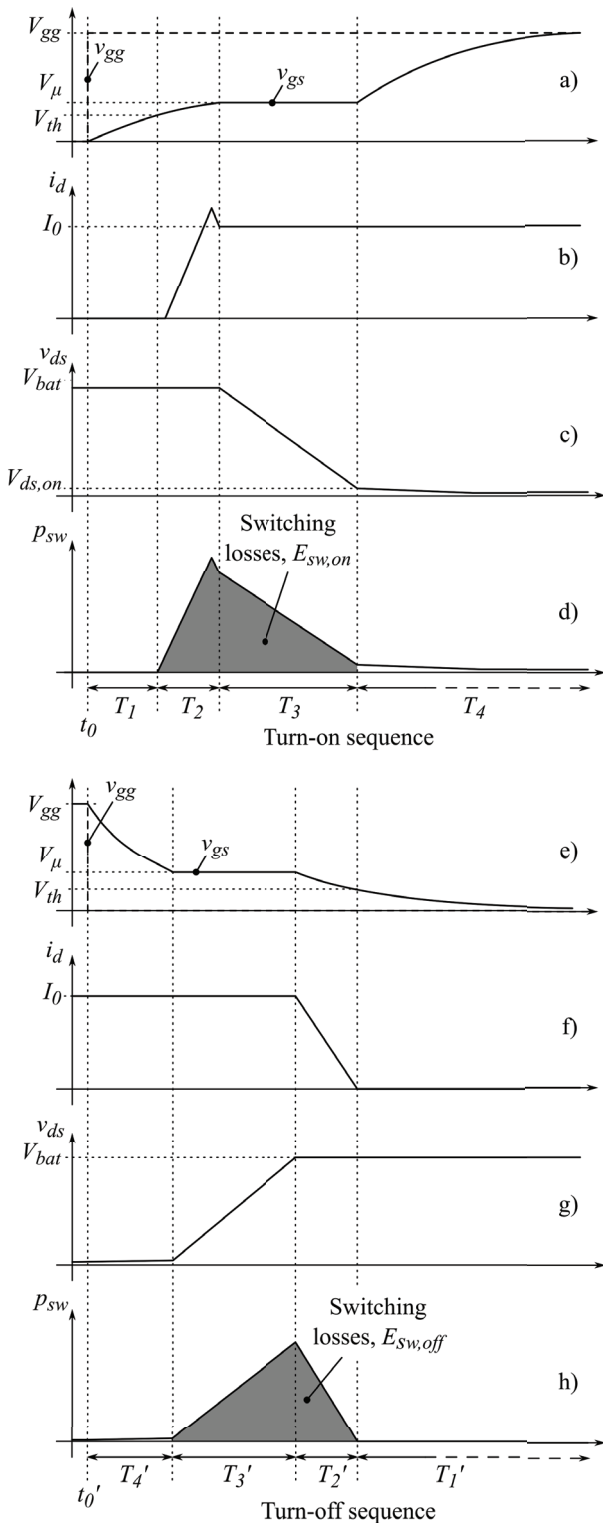


Figure 2: Switching sequence waveforms

### 3 Advanced gate control system

Figure 3 depicts the block diagram of the advanced gate control system presented in this paper. The system is constructed of two main units, namely the current sources unit and the control circuit unit. The role of the first is to feed the power MOSFET gate, while the second unit monitors the power MOSFET operating point, detects the ongoing switching sequence interval and produces control signals for the current sources unit. Each unit operation is explained in detail in the following sections.

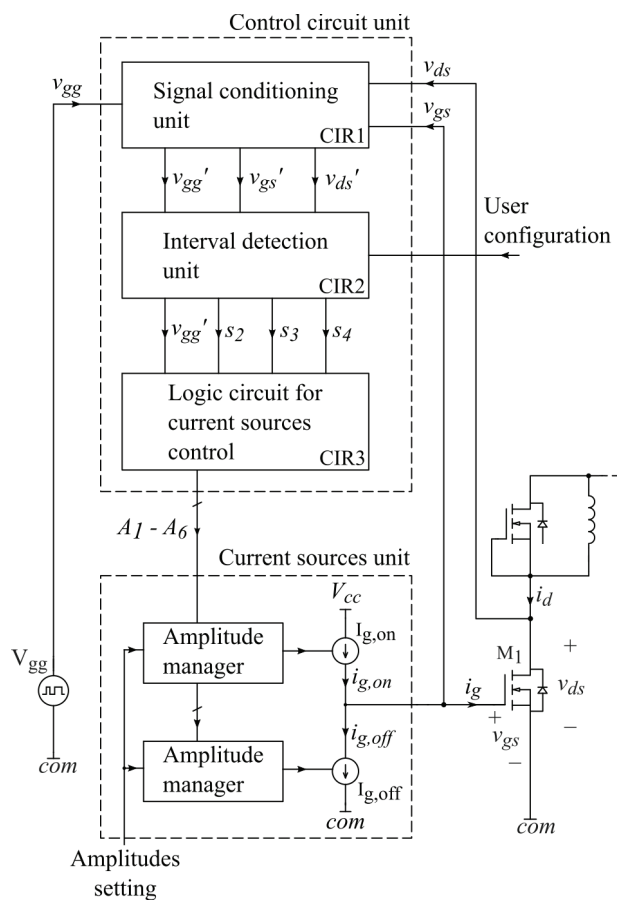


Figure 3: Advanced gate control system block diagram

#### 3.1 Current sources unit

The advanced gate control system (Figure 3) is based on the power transistor gate current shaping ( $i_g$ ) principle, implemented using two controlled current sources ( $I_{g,on}$  and  $I_{g,off}$ ) that charge and discharge the transistor input capacitance during its turn-on and turn-off. Each source amplitude can be individually set in each interval of the switching sequences.

By adjusting the gate current ( $i_g$ ) in each interval, the charge flow rate to the gate is governed and hence the rate of change of each interval transition can be indi-

vidually controlled. We can therefore adjust each current and voltage slope ( $di/dt$  and  $dv/dt$ ) in intervals  $T_2$ ,  $T_3$ ,  $T_2'$  and  $T_3'$  and also minimize turn-on and turn-off delays in  $T_1$  and  $T_4'$  and the duration of the final gate charging and discharging in the intervals  $T_4$  and  $T_1'$ . An example of the advanced gate control operation is shown in Figure 4.

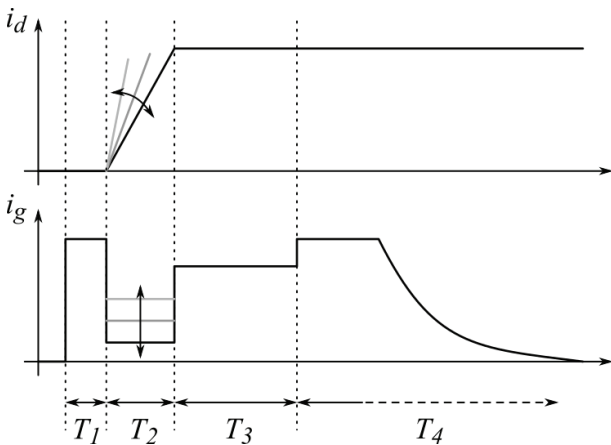


**Figure 4:** By shaping gate current  $i_g$  drain current slope is being controlled

The presented gate control approach can improve the conventional gate control drawback where all interval transitions are influenced simultaneously with  $R_g$  adaptation. Determining the optimal point of the trade-off between switching losses and electromagnetic emissions is thus much more effective. In most situations, less switching losses are produced for the same rate of electromagnetic emissions. Delays and final gate charging and discharging durations can also be minimized.

The  $i_g$  amplitude adjustment throughout the switching intervals is performed by the amplitude manager system. It enables the user to set the desired interval amplitude levels and control the  $I_{g,on}$  and  $I_{g,off}$  current sources. The operation of the amplitude manager is based on the information about the ongoing interval, which is obtained from the control circuit unit. Amplitude managers and current sources are implemented as current mirrors, described in detail in section 4.

The current sources are supplied with voltages ( $V_{cc}$ ) equal to gate-source voltage ( $v_{gs}$ ) required for power transistor full turn-on (typically 12V for common power MOSFETs).

### 3.2 Control circuit unit

The role of the control circuit unit is to detect borders between the intervals of the switching sequence and to subsequently send information about the ongoing

interval to the current sources block. It consists of three subunits, namely the signal conditioning unit (CIR1), interval detection unit (CIR2) and logic circuit for the current sources control (CIR3).

#### 3.2.1 Signal detection and Signal conditioning unit

The signal conditioning unit (CIR1) accepts signals  $v_{ds}$  and  $v_{gs}$  from the MOSFET and the control signal  $v_{gg}$  (usually from a microcontroller). To understand why it is necessary to monitor  $v_{ds}$  and  $v_{gs}$ , we must first take a look at the interval detection principle. The interval borders are associated with specific events, marked with points  $N_0, N_2, N_3$  and  $N_4$  for turn-on and  $F_0, F_4, F_3$  and  $F_2$  for turn-off in Figure 5 and explained in Table 1. As evident from Figure 5, the points are located on  $v_{ds}$ ,  $v_{gs}$  and  $v_{gg}$ , which means that these signals provide full information about the ongoing interval. It should be emphasized that the points are located exclusively on the voltage signals that are commonly present in each inductive load circuit. This is an important advantage of the presented system, as it enables an implementation in various power applications regardless of voltage or current rating.

**Table 1:** Interval border points explanation

Point	Start of interval	Associated event
$N_0$	$T_1$	Start of TURN-ON sequence, $v_{gg}$ starts rising
$N_2$	$T_2$	$v_{gs}$ reaches threshold voltage $V_{th}$
$N_3$	$T_3$	$v_{ds}$ starts falling
$N_4$	$T_4$	$v_{ds}$ drops to the final value
Power transistor is ON		
$F_0$	$T_4'$	Start of TURN-OFF sequence, $v_{gg}$ starts dropping
$F_4$	$T_3'$	$v_{ds}$ starts rising
$F_3$	$T_2'$	$v_{ds}$ rises to the final value
$F_2$	$T_1'$	$v_{gs}$ drops to the threshold voltage
Power transistor is OFF		

Before point sensing and interval detection, the input signals  $v_{ds}$  and  $v_{gs}$  are processed by the signal conditioning unit (Figure 6). Signals must be filtered first to eliminate high-frequency oscillations that commonly occur during the power transistor switching. The filters must be carefully designed to keep their time constant small compared to the switching sequence interval durations. The control signal  $v_{gg}$ , which is a logic signal, must be voltage-matched to meet the comparator input requirements.

#### 3.2.2 Interval detection unit

After filtering, the signals are passed to the interval detection unit (CIR2) that outputs the signals  $s_2$ ,  $s_3$  and  $s_4$

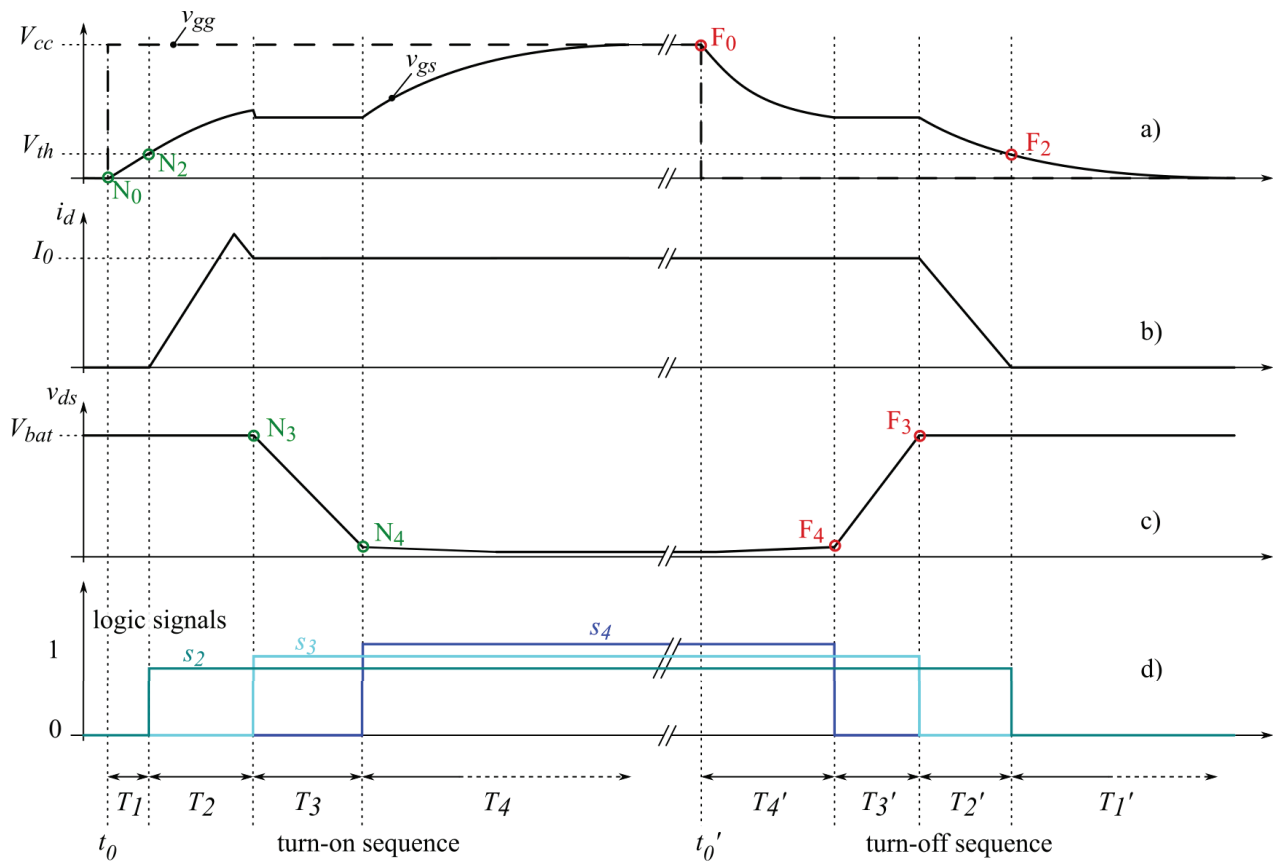


**Figure 5:** Switching sequence with N and F points

(Figure 5 d), which provide full information about the ongoing interval (by forming a unique combination in each interval) in conjunction with  $v_{gg}$ . Each of the three signals is set high and then low at two points:  $s_2$  at  $N_2$  and  $F_2$ ,  $s_3$  at  $N_3$  and  $F_3$ , and  $s_4$  at  $N_4$  and  $F_4$  respectively (Figure 5). Since each point pair detection and corresponding output signal generation follows the same principle and utilizes an identical circuit (depicted in Figure 7), a common explanation is applicable hereafter, where the input signal stands for  $v_{gs}'$  and  $v_{ds}'$  and the output signal for  $s_2$ ,  $s_3$  and  $s_4$ . For  $s_2$ , the input signal is  $v_{gs}'$ , while for  $s_3$  and  $s_4$  generation, the input signal is  $v_{ds}'$ . Since  $v_{gg}'$  is a logic signal, the detection of points  $N_0$

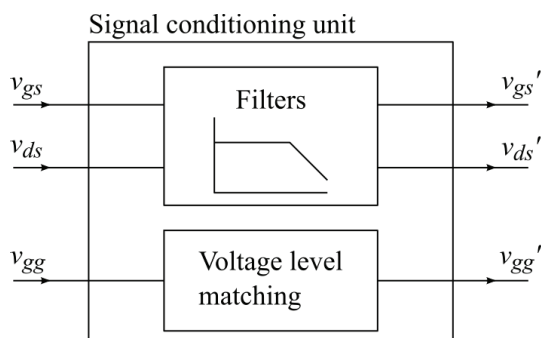


**Figure 6:** Signal conditioning unit (CIR1)

an  $F_0$  does not require utilizing the circuit from Figure 7. The  $v_{gg}'$  transition detection is carried out in the logic circuit for current sources control unit (CIR3).

As evident from Figure 7, the input signal  $v_{gs}'$  or  $v_{ds}'$  crossing a certain level at points  $N_i$  or  $F_i$  is sensed by the comparator ( $U_1$  and  $U_2$ ). The point levels are user-configured by adapting the input voltage dividers ( $R_1$ - $R_2$ ) and ( $R_3$ - $R_4$ ). In case that a voltage signal at a compara-

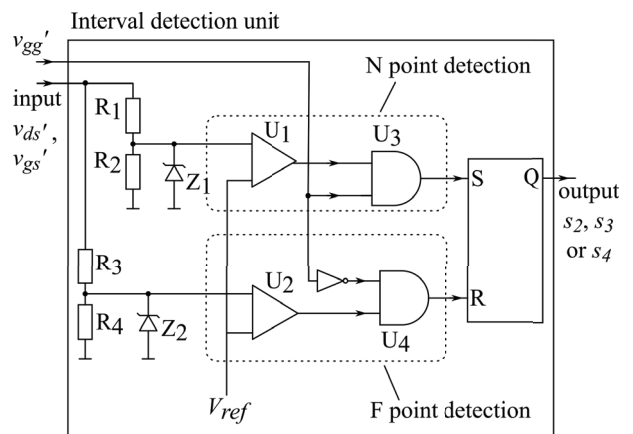


**Figure 7:** Interval detection unit (CIR2) – one out of three identical circuits is depicted.

tor input exceeds its rating, the Zener diodes  $Z_1$  and  $Z_2$  start clamping to protect the comparator inputs. To ensure that  $N_i$  and  $F_i$  points are detected exclusively during turn-on and turn-off sequences and to prevent flip-flop mistripping, the AND gates  $U_3$  and  $U_4$  with

applied  $v_{gg}'$  and  $\overline{v_{gg}'}$  inputs are inserted to generate a sequence-matching window for passing comparator output signal. When a point crossing is detected, a SR flip-flop input is triggered:  $S$  input at  $N_i$  and  $R$  input at  $F_i$  point detection, which generates a  $Q$  signal that matches the desired output signal waveforms  $s_{2'}$ ,  $s_3$  or  $s_{4'}$ , Figure 5.

Using flip-flops for the interval detection is also important to ensure the immunity to oscillations, as SR flip-flops react only on the first input triggering. Therefore, comparator input signal oscillation around  $V_{ref}$  (which results in comparator output alternating) has no effect on the  $s_{2'}$ ,  $s_3$  or  $s_{4'}$  waveforms.

### 3.2.3 Logic circuit for current sources control

The signals  $s_{2'}$ ,  $s_3$  and  $s_{4'}$  are passed to the logic circuit CIR3 (Figure 3) that together with the signal  $v_{gg}'$  produces the controlling signals  $A_1$  to  $A_6$  for the current sources unit. The operation of this unit follows the selected current sources control scheme, which is described in detail in the next section.

## 4 System implementation

The system is implemented as an IC in a 250 nm TSMC technology (Figure 10). The circuit integration is essential for an efficient system embodiment. First, it enables short propagation delay of the controlling circuit, which is crucial to be small in comparison to the interval durations allowing the management of switching transients. To make our system implementable in applications with expected switching transient durations of 100ns, it is considered that signal propagation delay must not exceed 10 ns, which is likely unachievable using discrete components. Furthermore, the integration allows an efficient realization of current sources and amplitude managers in the form of integrated current mirrors. An important integration benefit is also minimization of the system physical dimensions.

The purpose of the system implementation presented in this work is to prove the concept of the described system. In order to simplify the system development and future research, only the crucial parts are integrated. According to Figure 3, these are the current sources unit with the exception of resistors the  $R_{ref1}$  to  $R_{ref6}$  (Figure 8), logic circuitry for controlling current sources and the interval border detection unit with the exception of

input voltage dividers ( $R_1$ ,  $R_2$  and  $R_3$ ,  $R_4$  in Figure 7). The system is supplied with two voltage levels, 5 V for the controlling circuit and 12 V ( $V_{cc}$ ) for the current sources unit.

### 4.1 Current sources unit realization

Figure 8 presents a realization of the current sources unit with integrated current mirrors. The transistors  $M_{h0}$  and  $M_{l0}$  present a physical implementation of the current sources  $I_{g,on}$  and  $I_{g,off}$  (from Figure 3), while the rest of the circuit embodies the corresponding amplitude managers. The unit is divided into a high-side and low-side subcircuit, each consisting of three channels (two of them depicted dimmed) that enable setting different  $i_{g,on}$  and  $i_{g,off}$  amplitude levels and shape the gate current ( $i_g$ ) during switching sequence intervals.

The amplitude levels are user-defined by adjusting the  $R_{ref1}$  to  $R_{ref6}$  resistor values (not part of IC) that determine current mirror reference currents for each channel ( $i_{r1}$ ,  $i_{r2}$ ,  $i_{r3}$  and  $i_{r4}$ ,  $i_{r5}$ ,  $i_{r6}$ ). The reference currents are mirrored to  $i_{h2'}$ ,  $i_{h2''}$ ,  $i_{h2'''}$  and  $i_{l2'}$ ,  $i_{l2''}$ ,  $i_{l2'''}$ . A single mirror is required for the high side subcircuit, while the low side requires two mirroring stages for the  $I_{g,on}$  and  $I_{g,off}$  source and sink realization. The mirrored currents are then combined into  $i_{h1}$  and  $i_{l1}$  ( $i_{h1}=i_{h2}'+i_{h2}''+i_{h2}'''$  and  $i_{l1}=i_{l2}'+i_{l2}''+i_{l2}'''$ ) that present the reference currents for the  $M_{h1}$ - $M_{h0}$  and  $M_{l1}$ - $M_{l0}$  current mirrors and in turn determine the  $i_{g,on}$  and  $i_{g,off}$  waveforms. Each output current therefore consists of three components and can be defined as (3) and (4), where  $M$  indicates the total current mirror multiplication factor. In this design,  $M$  equals 1000.

$$i_{g,on}(t) = M \cdot i_{r1}(t) + M \cdot i_{r2}(t) + M \cdot i_{r3}(t) \quad (3)$$

$$i_{g,off}(t) = M \cdot i_{r4}(t) + M \cdot i_{r5}(t) + M \cdot i_{r6}(t) \quad (4)$$

To set the  $i_g$  amplitude in each interval separately, the transistors  $M_{h3'}$ ,  $M_{h3''}$ ,  $M_{h3'''}$  and  $M_{l3'}$ ,  $M_{l3''}$ ,  $M_{l3'''}$  are utilized, controlled by the  $A_1$  to  $A_6$  signals from the logic circuit for current sources control CIR3 (Figure 3). The transistors act as switches and take over the reference currents  $i_{r1}$  to  $i_{r6}$  from  $M_{h2'}$ ,  $M_{h2''}$ ,  $M_{h2'''}$  and  $M_{l2'}$ ,  $M_{l2''}$ ,  $M_{l2'''}$ . This causes zero current mirroring in the corresponding channels and consequently zero  $i_{h2'}$ ,  $i_{h2''}$ ,  $i_{h2'''}$ ,  $i_{l2'}$ ,  $i_{l2''}$  or  $i_{l2'''}$  contribution in the formation of the  $i_{h1}$  and  $i_{l1}$  currents, which, as presented, impact the  $i_{g,on}$  and  $i_{g,off}$  amplitudes.

To put it briefly, the gate current  $i_g$  shaping is embodied by the switching signals  $A_1$  to  $A_6$  throughout intervals which define the appropriate current components from the expressions (3) and (4) to form the  $i_{g,on}$  and  $i_{g,off}$  currents at a given time. The  $i_{g,on}$  and  $i_{g,off}$  amplitude levels are set by adjusting the reference currents by the external  $R_{ref1}$  to  $R_{ref6}$  resistors.

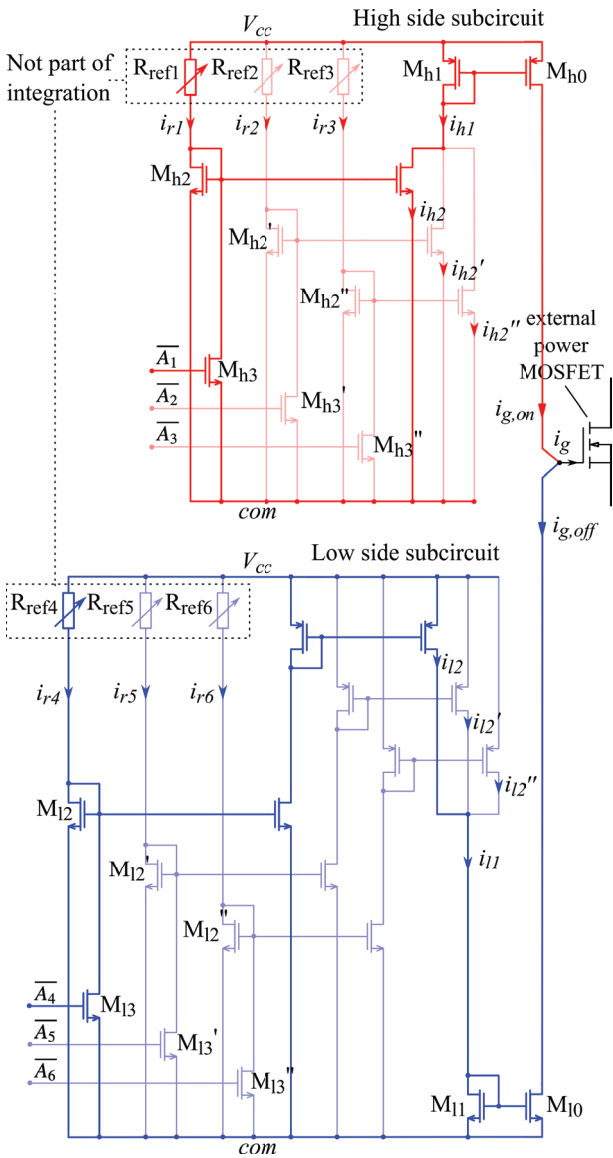


**Figure 8:** Schematic of current sources unit and corresponding amplitude managers (High side subcircuit for  $i_{g,on}$  and Low side subcircuit for  $i_{g,off}$ )

4.2 Current sources controlling scheme

In each interval, a particular  $A_1$  to  $A_6$  signal combination is provided by logic circuit for current sources control (CIR3) to ensure fast and smooth current shaping. The resulting  $i_{g,on}$  and  $i_{g,off}$  current composition of multiplied reference currents ( $M \cdot i_{r1}$  to  $M \cdot i_{r6}$ ) is presented in Figure 9.

As evident, the  $i_{g,on}$  and  $i_{g,off}$  components  $M \cdot i_{r2}$  and  $M \cdot i_{r6}$  are present during the whole turn-on and turn-off sequences. Regarding the turn-on, in the intervals  $T_1$  and  $T_4$   $M \cdot i_{r1}$  is added to  $M \cdot i_{r2}$  to minimize the delay and final gate charging duration. During  $T_2$  only  $M \cdot i_{r2}$  is available – the power transistor current slope is usually the one requiring the strongest mitigation and therefore re-

quires the lowest gate current. The voltage slope in  $T_3$  is managed by  $M \cdot i_{r2}$  and  $M \cdot i_{r3}$ .

A similar operation refers to the turn-off:  $M \cdot i_{r6}$  and  $M \cdot i_{r4}$  in  $T_4'$  minimize the turn-off delay, and  $M \cdot i_{r6}$  and  $M \cdot i_{r5}$  determine the voltage slope in  $T_3'$ . Only  $M \cdot i_{r6}$  component is present during the current transition in  $T_2'$ . Since the duration of the input capacitances discharging in  $T_1'$  is already limited by the low power transistor  $v_{gs}$  voltage and intrinsic resistances, only the  $M \cdot i_{r6}$  component is provided.

During the turn-on sequence,  $i_{g,off}$  equals zero, and similarly,  $i_{g,on}$  equals zero during the turn-off.

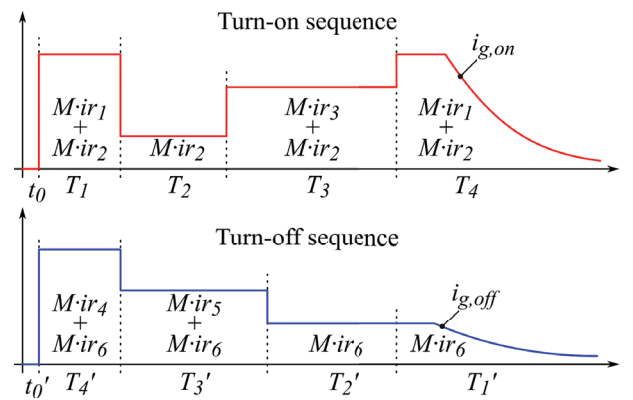


**Figure 9:** composition of  $i_{g,on}$  and  $i_{g,off}$  currents

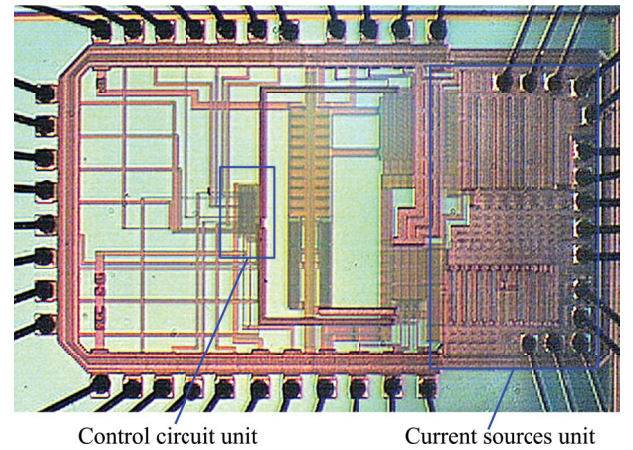


**Figure 10:** A microphotograph of the advanced gate control ASIC. IC dimensions approx. 1502  $\mu\text{m}$  x 2430  $\mu\text{m}$

5 Testing, results and discussion

5.1 Test setup

To investigate the efficiency, the advanced gate control system is compared to the conventional control method with the series gate resistance. The test is carried out using a common inductive load circuit, as depicted



in Figure 11 (the circuit basic operation is already described in Section 1). Between the gate and the source terminals of MOSFET  $M_1$ , a 10 kΩ resistor and a 10 nF capacitor are inserted to emulate realistic conditions. The two components are often inserted in power circuits to improve immunity against unintentional turn-on and to mitigate the Miller effect consequences. MOSFET  $M_1$  can be driven with the advanced or conventional control method, while the drain-source voltage ( $v_{ds}$ ), the gate-source voltage ( $v_{gs}$ ) and the drain current ( $i_d$ ) are monitored with the oscilloscope. To measure the  $i_d$  current, a Rogowski coil is utilized. The MOSFETs  $M_1$  and  $M_2$  are both Infineon IPB010N06N.

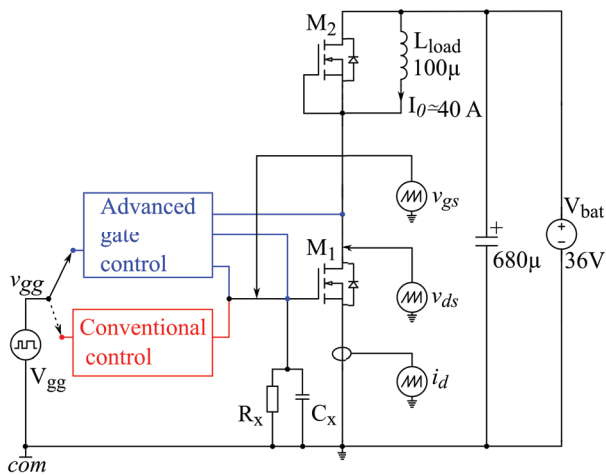


**Figure 11:** The test circuit schematics

The waveform generator  $V_{gg}$  (Agilent 33500B) is programmed to produce a pulse shown in Figure 12. During the interval  $T_{charge}$ ,  $M_1$  is open. In this interval, the current through  $L_{load}$  rises up to the desired value  $I_0$  in this case 40 A. After that,  $M_1$  is switched off and  $i_d$  is diverted into  $M_2$ 's diode, which produces the required initial conditions to observe the turn-on and turn-off switching sequences at the following  $v_{gg}$  fronts. The time be-

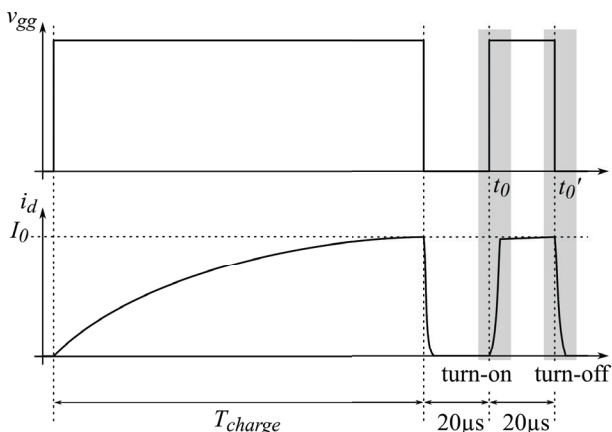


**Figure 12:**  $v_{gg}$  and corresponding  $i_d$  waveforms

tween the last three changes of  $v_{gg}$  is kept low (20  $\mu$ s) to produce only minimal change in  $i_d$ .

The advanced gate control from Figure 11 as such is described in previous sections. In the signal conditioning unit, first order low-pass filters are employed comprising of 10 kΩ resistor and 1 pF MLCC capacitor. Resistors  $R_{ref1}$  to  $R_{ref6}$  are trimmer potentiometers with 2 MΩ track resistance. The conventional control is composed of a special driver (IR AUIRS2191S) and the series gate resistor  $R_g$ .

The efficiency of the two methods is observed by comparing turn-on and turn-off switching losses, delays, and final charging / discharging durations at different values of the drain current rise or fall time. This figure of merit is chosen, as the current transitions are considered the most critical, since they are usually faster than voltage transitions and their mitigation produces greatest amount of surplus switching losses. Moreover, the comparison of current rise and fall times are more accurate, since the current transitions are not affected by parasitic elements in such extent as the voltage transitions.

Definitions of the observed parameters are shown in the Table 2.

**Table 2:** Parameters definitions

Parameter	Definition
Current rise time ( $t_{id,rise}$ )	$i_d=10\% I_0$ to $i_d=90\% I_0$
Current fall time ( $t_{id,fall}$ )	$i_d=90\% I_0$ to $i_d=10\% I_0$
Voltage rise time ( $v_{ds,rise}$ )	$v_{ds}=10\% V_{bat}$ to $v_{ds}=90\% V_{bat}$
Voltage fall time ( $v_{ds,fall}$ )	$v_{ds}=90\% V_{bat}$ to $v_{ds}=10\% V_{bat}$
Turn-on delay	$v_{gs}=10\% V_{cc}$ to $i_d=10\% I_0$
Turn-off delay	$v_{gs}=90\% V_{cc}$ to $v_{ds}=10\% V_{bat}$
Turn-on final charging	$v_{ds}=10\% V_{bat}$ to $v_{gs}=90\% V_{cc}$
Turn-off final discharging	$i_d=10\% I_0$ to $v_{gs}=10\% V_{cc}$
Turn-on switching losses ( $E_{sw,on}$ )	$E_{sw,on} = \int_{t_1}^{t_2} i_d v_{ds} dt$ $t_1$ when $i_d=10\% I_0$ $t_2$ when $v_{ds}=10\% V_{bat}$
Turn-off switching losses ( $E_{sw,off}$ )	$E_{sw,off} = \int_{t_1}^{t_2} i_d v_{ds} dt$ $t_1$ when $v_{ds}=10\% V_{bat}$ $t_2$ when $i_d=10\% I_0$

5.2 Measurements and results

Figure 13 first shows an example of the advanced gate control operation. The graphs present three turn-on switching sequence waveforms ( $i_d$ ,  $v_{ds}$  and  $v_{gs}$ ). Each time a different setting for  $i_{ref3}$  is applied (by adjusting  $R_{ref3}$  trimmer resistor) in order to manipulate  $v_{ds}$  fall time. Specifically, the  $i_{ref3}$  current is set to 1.7 mA, 706  $\mu$ A and 63  $\mu$ A, while the currents  $i_{ref1}$  and  $i_{ref2}$  are constant in all three cases and set to 370  $\mu$ A and 39  $\mu$ A respectively. It should be noted that the voltage drop that occurs during the current transition (while  $M \cdot i_{r2}$  is active) is a consequence of the voltage induction on parasitic inductances due to the relatively high  $di/dt$  rate being present and cannot be manipulated with the advanced gate control system. However, the last part of  $v_{ds}$  drop that can be influenced clearly underlines the system key advantage. While keeping the drain current rise time constant (at around 200 ns), the voltage drop rate could be boosted (in regards to the emission generation) thus reducing switching losses.

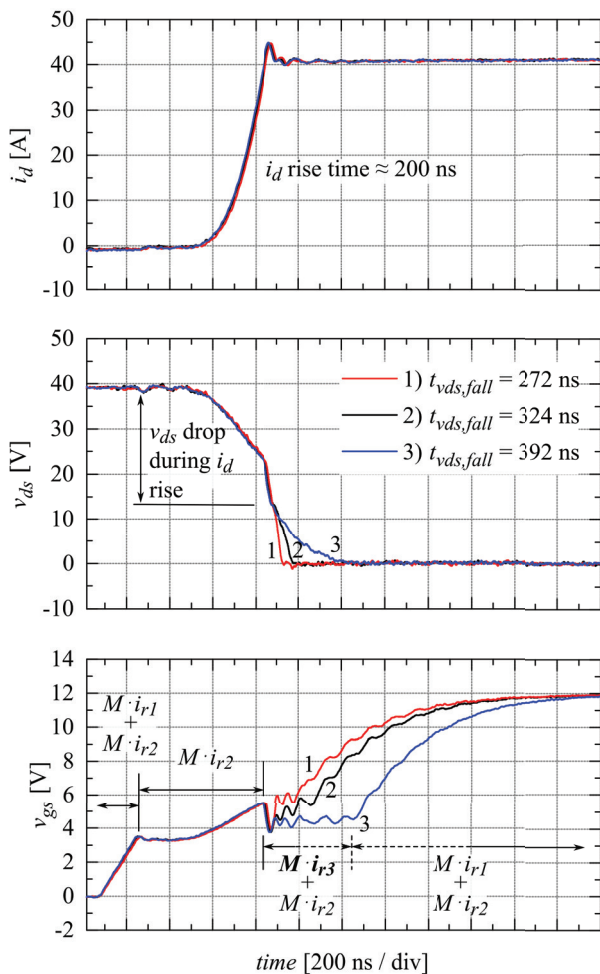


**Figure 13:** Advanced gate control operation, turn-on sequence oscillograms. Different  $t_{v_{ds},fall}$  are applied at the same  $t_{i_d,rise}$ .

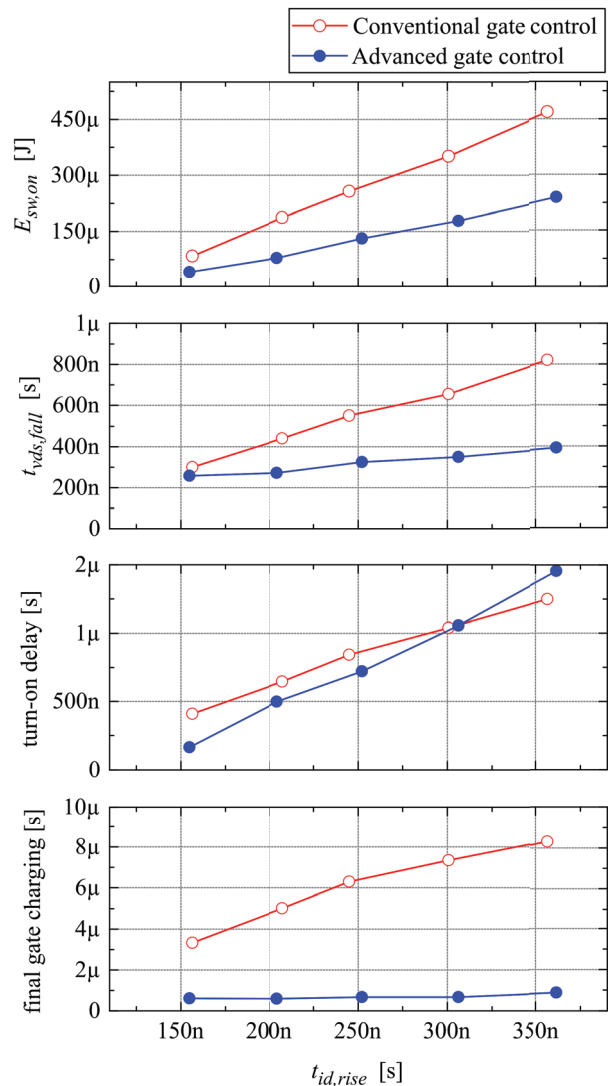


**Figure 14:** Comparison of the conventional and the advanced gate control methods, turn-on

To compare the two methods, the efficiency measurements are performed first with the conventional gate driving method using different gate resistor  $R_g$  values. For the turn-on, 39  $\Omega$ , 68  $\Omega$ , 90  $\Omega$ , 120  $\Omega$  and 150  $\Omega$  are used, which results in the following  $i_d$  rise times: 156 ns, 208 ns, 245 ns, 300 ns and 357 ns respectively. Similarly, for the turn-off, 47  $\Omega$ , 82  $\Omega$ , 100  $\Omega$ , 120  $\Omega$  and 150  $\Omega$   $R_g$  values are applied, producing 141 ns, 201 ns, 246 ns 277 ns and 346 ns  $i_d$  fall times. The corresponding turn-on and turn-off parameters from Table 2 are obtained by processing waveforms acquired from the oscilloscope.

Similar measurement is carried out using the advanced gate control system. This time, trimmer resistors  $R_{ref1}$  to  $R_{ref3}$  for the turn-on and  $R_{ref4}$  to  $R_{ref6}$  for the turn-off from Figure 8 are adjusted to manipulate switching sequence transitions. Such resistor values are chosen that  $v_{ds}$  rise and fall times, delays and final charging and dis-

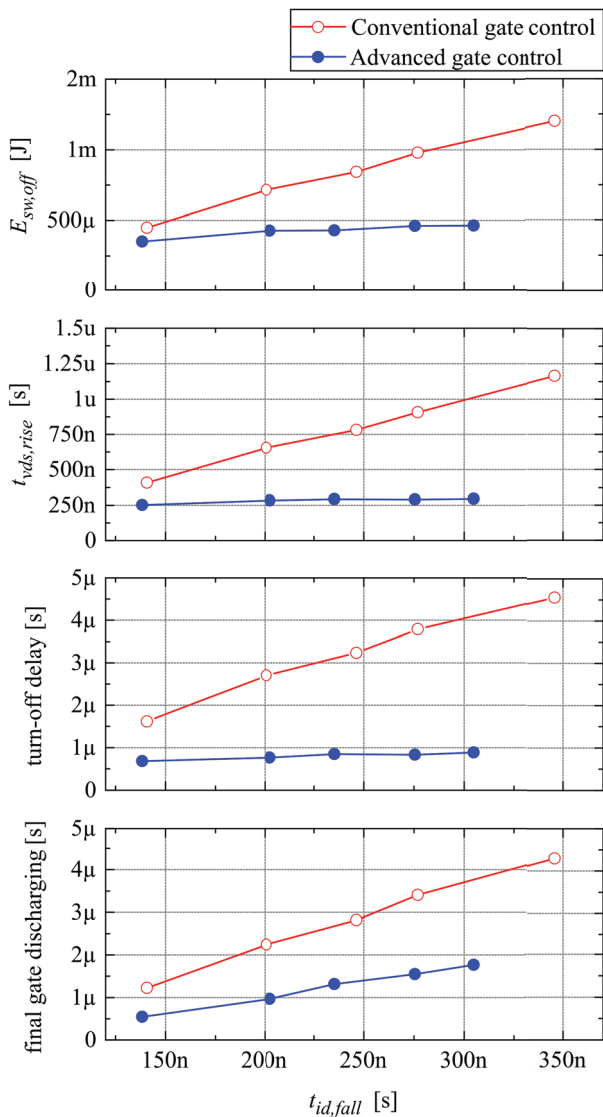


**Figure 15:** Comparison of the conventional and the advanced gate control methods, turn-off

charging durations are kept as low as possible, while  $i_d$  rise and fall times are matched to the values obtained using  $R_g$  control method. Again, turn-on and turn-off parameters from Table 2 are obtained by processing waveforms acquired from the oscilloscope.

The results of the comparison of the two methods are presented in Figure 14 and Figure 15.

Figure 14 and Figure 15 show that the extending drain current ( $i_d$ ) rise and fall times produce notably less switching losses, shorter turn-off delay and shorter final charging and discharging durations when using the advanced gate control. Switching losses reduction is in this case a consequence of keeping  $v_{ds}$  rise and fall time as small as possible.

The only parameter without a significant improvement is the turn-on delay, where the results of both methods are comparable. The reason for the advanced control method to be inefficient in this case is presumably the fact that the low reference current  $i_{r2}$  must first charge parasitic capacitances formed by connections on the test PCB and bond pads. This delays the establishment of adequate conditions in current mirrors in interval  $T_2$  for proper mirroring (in which only  $M \cdot i_{r2}$  is supposed to form  $i_{g,on}$ ). This causes that the current  $i_{g,on}$  to equal zero for a period of time, resulting in  $i_d$  current rise delay. The described effect is also evident in Figure 13. Just after  $M \cdot i_{r1} + M \cdot i_{r2}$  are active, there is a period of  $v_{gs}$  stagnation, which is a consequence of zero  $i_{g,on}$ . It is considered that the full integration of the amplitude manager (by using a different method for reference current setting instead of external  $R_{ref1}$  to  $R_{ref6}$  resistors) would eliminate the described problem.

## 6 Conclusion

The presented advanced gate control method efficiently reduces switching losses, as well as enables the minimization of the turn-off delay and final charging and discharging durations. This conclusion is obtained by comparing the advanced gate control with the conventional method. For illustration, in case of setting MOSFET drain current rise and fall times to 250 ns, the switching losses reduction is approximately 50% for turn-on and turn-off. Furthermore, the delays are reduced for 15% (turn-on) and 240% (turn-off), the turn-off final gate discharging duration is reduced for 50% while the turn-on final gate charging is as much as 10 times shorter. The system effectiveness increases with the current or voltage slope mitigation rate. The novel gate driving approach is thus proven effective.

The described method is applicable in a broad spectrum of applications, since it requires only to monitor the drain-source and gate-source voltages of the controlled MOSFET. The applications which would most significantly benefit from using the presented system are those where the switching losses dominate in the overall system losses, i.e. the applications with high switching frequency and/or high voltage and current ratings.

## 7 References

1. X. Wang, Y. Sun, T. Li, and J. Shi, "Active closed-loop gate voltage control method to mitigate metal-oxide semiconductor field-effect transistor turn-

- off voltage overshoot and ring," *IET Power Electron.*, vol. 6, no. 8, pp. 1715–1722, Sep. 2013.
2. B. Wittig and F. W. Fuchs, "Analysis and Comparison of Turn-off Active Gate Control Methods for Low-Voltage Power MOSFETs With High Current Ratings," *IEEE Trans. Power Electron.*, vol. 27, no. 3, pp. 1632–1640, Mar. 2012.
  3. M. Rose, J. Krupar, and H. Hauswald, "Adaptive  $dv/dt$  and  $di/dt$  control for isolated gate power devices," in *2010 IEEE Energy Conversion Congress and Exposition (ECCE)*, 2010, pp. 927–934.
  4. J. E. Makaran, "Gate Charge Control for MOSFET Turn-Off in PWM Motor Drives Through Empirical Means," *IEEE Trans. Power Electron.*, vol. 25, no. 5, pp. 1339–1350, May 2010.
  5. N. Idir, R. Bausiere, and J. J. Franchaud, "Active gate voltage control of turn-on  $di/dt$  and turn-off  $dv/dt$  in insulated gate transistors," *IEEE Trans. Power Electron.*, vol. 21, no. 4, pp. 849–855, Jul. 2006.
  6. S. Park and T. M. Jahns, "Flexible  $dv/dt$  and  $di/dt$  control method for insulated gate power switches," *IEEE Trans. Ind. Appl.*, vol. 39, no. 3, pp. 657–664, May 2003.
  7. H. P. Yee, "An EMI suppression MOSFET driver," in *Applied Power Electronics Conference and Exposition, 1997. APEC '97 Conference Proceedings 1997., Twelfth Annual, 1997*, vol. 1, pp. 242–248 vol.1.
  8. H.-G. Lee, Y.-H. Lee, B.-S. Suh, and D. Hyun, "An improved gate control scheme for snubberless operation of high power IGBTs," in *Conference Record of the 1997 IEEE Industry Applications Conference, 1997. Thirty-Second IAS Annual Meeting, IAS '97, 1997*, vol. 2, pp. 975–982 vol.2.
  9. S. Musumeci, A. Raciti, A. Testa, A. Galluzzo, and M. Melito, "Switching-behavior improvement of insulated gate-controlled devices," *IEEE Trans. Power Electron.*, vol. 12, no. 4, pp. 645–653, Jul. 1997.
  10. Y. Lobsiger and J. W. Kolar, "Closed-loop IGBT gate drive featuring highly dynamic  $di/dt$  and  $dv/dt$  control," in *2012 IEEE Energy Conversion Congress and Exposition (ECCE)*, 2012, pp. 4754–4761.
  11. B. J. Baliga, *Power semiconductor devices*. Boston: PWS Pub. Co., 1996.
  12. P. Haaf and J. Harper, "Understanding Diode Reverse Recovery and its Effect on Switching Losses," Fairchild Power Seminar 2007, 2007.
  13. D. A. Grant and J. Gowar, *Power MOSFETS: theory and applications*. New York: Wiley, 1989.
  14. B. Carsten and B. Mammano, "Understanding and Optimizing Electromagnetic Compatibility in Switchmode Power Supplies," Texas Instruments, 2003.

Arrived: 21. 10. 2016

Accepted: 29. 11. 2016